Asian Journal of Chemistry; Vol. 36, No. 4 (2024), 865-878

ASIAN JOURNAL OF CHEMISTRY

https://doi.org/10.14233/ajchem.2024.31150

In silico Studies of Cilnidipine Degradation Products for Structure Confirmation, Toxicity Prediction and Molecular Docking

KRISHNAM RAJU CHINTALAPATI[1,2], YESUDAS KADA[3], VASAVI MALKHED[4], SANATH KUMAR GOUD PALUSA[2], RABIN BERA[3] and V. SHANMUKHA KUMAR JAGARLAPUDI[1,*]

[1]Department of Chemistry, Koneru Lakshmaiah Education Foundation, Green Fields, Vaddeswaram-522302, India
[2]Analytical Research and Development, United States Pharmacopeial Convention - India (P) Ltd., Hyderabad-500101, India
[3]Synthetics Department, United States Pharmacopeial Convention - India (P) Ltd., Hyderabad-500101, India
[4]Molecular Modelling Research Laboratory, Department of Chemistry, University College of Science, Osmania University, Tarnaka, Hyderabad-500007, India

*Corresponding author: E-mail: shanmukh_fed@kluniversity.in

Received: 4 January 2024; *Accepted*: 24 February 2024; *Published online*: 30 March 2024; AJC-21584

In this study, a comprehensive analysis of cilnidipine and its degradation products (**KD1-KD4** and **CD1-CD3**) with three main objectives *viz*. (i) toxicity prediction for bacterial mutagenicity, (ii) assessment of pharmacological activity and (iii) density functional theory (DFT) calculations were performed for structure confirmation. For bacterial mutagenicity prediction, *in silico* assessments were performed following ICH M7 guidelines. Using rule-based and statistical-based methodologies, predictions revealed an alerting group in **CD1-CD3**, while no alerting group was observed in **KD1-KD4** for bacterial mutagenicity. To assess pharmacological activity, docking studies were conducted to identify the mode of binding and interaction types of cilnidipine and its degradation products with N-type and L-type calcium channel subunits 7VFS and 7UHF, respectively. Additionally, 20 drugs acting as calcium channel blockers were considered for docking analysis to correlate the affinities of binding. The interaction energies revealed that molecule **CD3** shows the highest binding affinity with the ligand molecules, with a binding energy of -9.2 (kcal/mol) with 7VFS and -8.7 (kcal/mol) with 7UHF proteins, followed by **KD3** with a binding energy of -8.7 (kcal/mol) (7VFS) and -7.9 (kcal/mol) (7UHF). Furthermore, DFT calculations were employed to reassess the structures of degradation products **CD1** and **CD2** proposed in the literature. Simulating ^{1}H and ^{13}C NMR spectra, the obtained data demonstrated good agreement with experimental results, confirming the proposed stereo-configurations in the literature. Based on *in silico* bacterial mutagenicity predictions and docking studies, **KD3** emerged as a promising compound for receptor binding. Additionally, DFT calculations provided structural insights, affirming stereo-configurations proposed in the existing literature. This multifaceted approach contributed valuable insights into the toxicity, pharmacology and structural aspects of cilnidipine degradation products.

Keywords: Cilnidipine, Degradation products, Density functional theory, Toxicity predictions, Docking study.

INTRODUCTION

Cilnidipine is a dihydropyridine calcium channel blocker with both L-type and N-type blocking functions [1]. The degradation studies of a drug are of utmost importance for identifying potential drug impurities. Degradation analysis were conducted on cilnidipine in our earlier work and seven products were identified, including **KD1** to **KD4** and **CD1** to **CD3**, as shown in Fig. 1 [2]. The toxicity of these degradation products remains unknown. However, according to regulatory guidelines [3], the assessment and control of mutagenic impurities in pharmaceuticals are crucial to limit the potential carcinogenic risk. Further, the guidelines recommended to predict bacterial mutagenicity for all possible impurities in the drug substance [4-6]. This prompted us to extend the study to predict the bacterial mutagenicity of these degradants using *in silico* tools. As these degradation products closely related to cilnidipine chemical structure, it is noteworthy to investigate their binding affinities to identify new leads for drug discovery. Hence, docking studies were conducted for these degradation products along with the existing drug molecules with the receptor protein. Among the seven degradation products, **CD1** and **CD2** exhibit five chiral

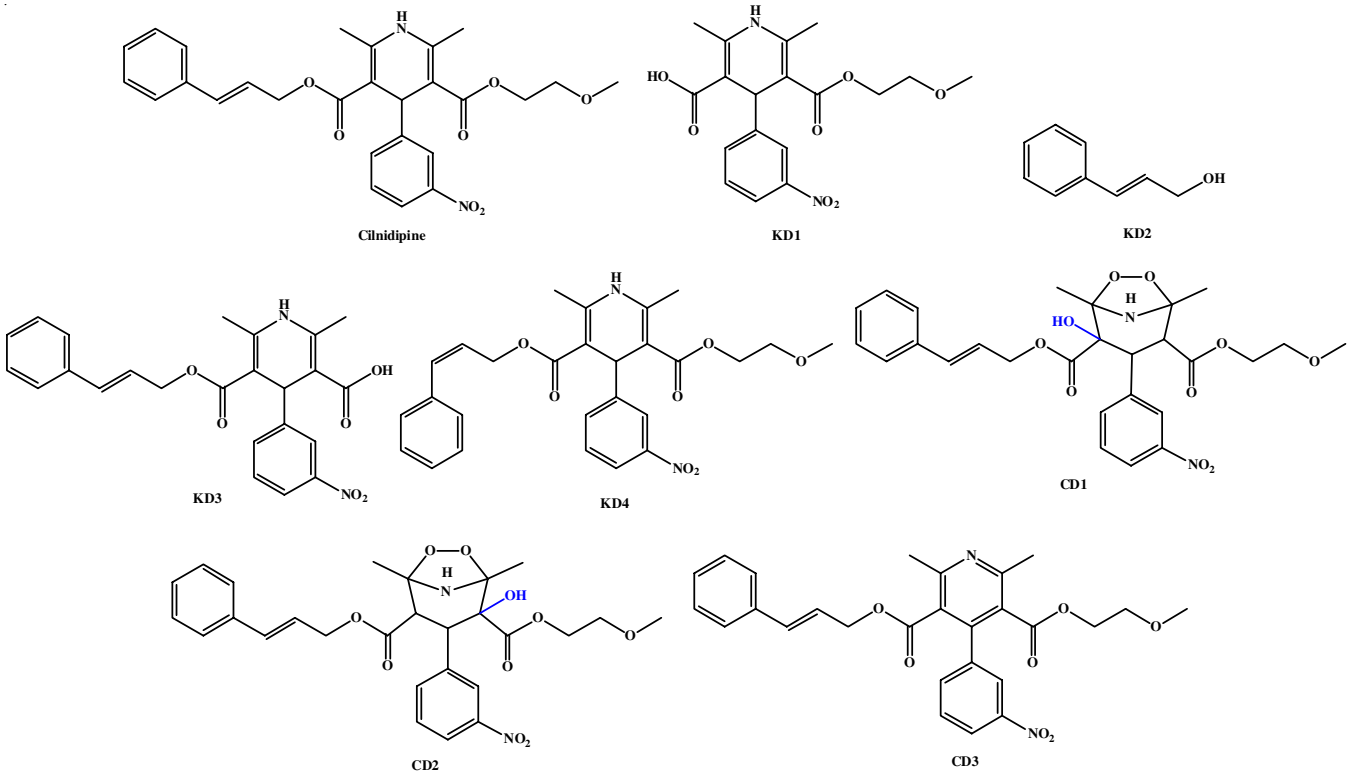

Fig. 1. Chemical structures of cilnidipine and its degradation products

centers each. The stereochemistry for these two structures was initially proposed based on NMR studies. In the present study, the stereo assignments of five chiral carbon atoms in both **CD1** and **CD2** were revisited using the *in silico* tools. This comprehensive approach contributes to a better understanding of the potential bacterial mutagenicity, pharmacological activity and structural aspects of cilnidipine and its degradation products.

EXPERIMENTAL

Toxicity prediction: Cilnidipine and its degradation products (**KD1** to **KD4** and **CD1** to **CD3**) are being considered for bacterial mutagenicity predictions in accordance with ICH M7 guidelines. Two complementary *in silico* methodologies were employed, utilizing both rule-based and statistical based approaches. Specifically, Derek Nexus (Version: 6.2.1, Lhasa Limited) was used for rule-based toxicity prediction, while Sarah Nexus (Version: 3.2.1, Lhasa Limited) was employed for statistical-based toxicity prediction. The chemical structures of individual cilnidipine and its degradation products (**KD1** to **KD4** and **CD1** to **CD3**) were formatted in ".cdx" and uploaded individually to the Derek Nexus software. Derek Nexus, capable of predicting toxicity for various endpoints, was configured to predict bacterial mutagenicity by selecting "bacterium" as species and "mutagenicity" as endpoint. Prediction outcomes from Derek Nexus include categories ranging from certain, plausible, probable, equivocal, doubted, improbable, to impossible and inactive, representing a spectrum from positive to negative predictions. Similarly, the chemical structures were uploaded to the Sarah Nexus software, which specializes in bacterial mutagenicity prediction under a statistical methodology. Sarah Nexus general prediction outcomes encompass positive, negative, equivocal and out-of-domain results. This dual approach provides a comprehensive assessment of the bacterial mutagenicity potential of cilnidipine and its degradation products.

Molecular docking: The Autodock vina software [7] with the PyRx interface is used for the docking of cilnidipine and its degradation products. Additionally, several drug molecules functioning as calcium channel blockers are also subjected to docking with the receptor protein molecule. Protein molecules, specifically N-type and L-type calcium channel proteins, along with 20 calcium channel blocker drugs, cilnidipine and its degradation products are subjected to docking in pdbqt format. A grid is generated at the active site, which corresponds to the ligand binding site or the calcium channel region of the proteins. The resulting docked complexes are visually inspected using the Biovia discovery studio visualizer 2021 (BIOVIA, Dassault Systems, Discovery studio visualizer, San Diego: 2021).

Structure confirmation of CD1 and CD2: CD1 and **CD2:** The structure of these products were re-examined computationally to correct or to support the originally proposed stereo-configuration around the five-carbon nucleus. The calculations have been performed using the Gaussian 09 *ab initio*/DFT quantum chemical program [8]. The gas phase molecular geometries of all the possible diastereomers were fully energy minimized without any symmetry constraints. The geometries were obtained with minimal potential energy surface, characterized by the real values for vibrational frequencies at the same Hessian. Gauge independent atomic orbital (GIAO) [9] approximation is used for the calculation of isotropic ^{1}H and ^{13}C NMR shielding constants. This theoretical model provides accurate chemical

shift values with less computational time. The equilibrium solvation effects for DMSO were considered by employing self-consistent reaction field (SCRF) method in combination with the conductor-like polarizable continuum model (C-PCM) [10, 11]. The chemical shifts were then calculated as $\delta = \sigma_{ref} - \sigma$, where TMS was used as reference and the shielding constant (σ_{ref}) was obtained by using the same level of theory (σ_{ref} = 31.6493 ppm and 193.3292 ppm, respectively for ^{1}H and ^{13}C atoms). All the calculations were performed using the hybrid DFT-B3LYP functional [12] in combination with 6-31+G-(d,p) basis set.

To compare the calculated data with the experimental results, a linear fit of calculated *versus* experimental shifts ($\delta_{calc} = a + b\delta_{exp}$) the intercept a, the slope b and the correlation coefficient R^2 is obtained. The obtained values were evaluated in terms of MAE (mean absolute error) = $\Sigma_n|\delta_{calc} - \delta_{exp}|/n$, CMAE (corrected mean absolute error) = $\Sigma_n|\delta_{scaled} - \delta_{exp}|/n$, where $\delta_{scaled} = (\delta_{calc} - a)/b$ measures the difference between the experimental and the predicted values by the linear fitting, MaxE (maximum error) = $\max(|\delta_{calc} - \delta_{exp}|)$ and CMaxE (corrected maximum error) = $\max(|\delta_{scaled} - \delta_{exp}|)$. Collectively, these statistical parameters show how close the computed values are with the experimental values. This also judge the accuracy of the computational protocol. During the statistical analysis, the labile protons (NH and OH) are excluded from the correlation, which would minimize the statistical parameters and highlight the differences in the region of interest for the comparison. It is also observed that the sources of variance in the calculated chemical shifts like conformational degrees of freedom in 2-methoxy ethyl formate, cinnamyl formate and nitrobenzene groups attached to the core bicyclic skeleton and flexibility of hydroxyl groups were neglected.

RESULTS AND DISCUSSION

Toxicity prediction results: QSAR methodologies are employed to predict the bacterial mutagenicity potential of cilnidipine and its degradation products (**KD1** to **KD4** and **CD1** to **CD3**) [13-16]. Cilnidipine and its degradation products, **KD1** to **KD4**, resulted in a negative prediction for bacterial mutagenicity (Table-1). On the other hand, the remaining degradation products, **CD1** to **CD3**, are predicted to be positive for bacterial mutagenicity using QSAR methodologies (Table-1).

TABLE-1
BACTERIAL MUTAGENICITY PREDICTION RESULTS FOR CILNIDIPINE AND ITS DEGRADANTS (**KD1** TO **KD4** AND **CD1** TO **CD3**)

Molecule	Toxicity prediction results		
	Derek Nexus (rule based)	Sarah Nexus (statistical based)	Conclusion
Cilnidipine	Inactive	Negative	Negative
KD1	Inactive	Negative	Negative
KD2	Inactive	Negative	Negative
KD3	Inactive	Negative	Negative
KD4	Inactive	Negative	Negative
CD1	Plausible	Out of domain	Positive
CD2	Plausible	Out of domain	Positive
CD3	Plausible	Negative	Positive

Derek Nexus software predicted plausible outcomes for **CD1** and **CD2** structures due to the presence of an aromatic nitro group, which is considered an 'alerting structure'. Similarly, Sarah Nexus made a positive hypothesis for these structures based on the aromatic nitro group. However, Sarah Nexus could not make an overall prediction because of the presence of a bicyclic group, falling outside its applicability domain. Consequently, the prediction for **CD1** and **CD2** structures by Sarah Nexus was considered out of domain. The overall *in silico* prediction for **CD1** and **CD2** structures is concluded as positive (Table-1). For **CD3** structure, Derek Nexus predicted positivity due to the presence of an aromatic nitro compound. While Sarah Nexus generated an overall negative prediction, however one positive hypothesis (aromatic nitro group) has been identified. Therefore, the Sarah Nexus negative prediction was over-ruled and an overall *in silico* prediction was considered positive for **CD3** structure (Table-1). These positive *in silico* predictions need further confirmation through experimental testing to ascertain the actual mutagenic potential of these compounds.

The chemical structures of cilnidipine, **KD1**, **KD3** and **KD4** contain an aromatic nitro group, which is considered an "alerting structure" that might raise concerns for potential mutagenicity. Despite the presence of the aromatic nitro group, Derek Nexus predicted these structures as negative for mutagenicity. The reason for this negative prediction is mentioned as the presence of dihydropyridine substituted nitrobenzenes. This suggests that the specific dihydropyridine substitution pattern on the nitrobenzene rings may counteract the mutagenic potential of the aromatic nitro group. Sarah Nexus also resulted in a negative prediction for these structures. The negative prediction is attributed due to the more relevant training set structures containing dihydropyridine substituted nitrobenzenes, which had a negative call for mutagenicity. Based on both Derek Nexus and Sarah Nexus predictions being negative, the *in silico* mutagenicity prediction for cilnidipine, **KD1**, **KD3** and **KD4** structures is concluded as negative (Table-1). This means that these structures are not predicted to be mutagenic according to the models used in Derek Nexus and Sarah Nexus.

Derek Nexus did not show any alert for the **KD2** structure, it resulted in a negative prediction for mutagenicity. On the other hand, Sarah Nexus, having **KD2** structure in its training data set with a negative call for mutagenicity, produced a certain negative prediction for the **KD2** structure. The overall *in silico* mutagenicity prediction for the **KD2** structure is concluded as negative (Table-1).

Molecular docking studies: The protein voltage-dependent N-type calcium channel subunit alpha 1B with PDB ID 7VFS_a and Voltage-dependent L-type calcium channel subunit alpha-1D with PDB ID 7UHF are used as a target proteins for docking studies [17,18]. Cilnidipine molecule and its degradation product (**CD1** to **CD3** and **KD1** to **KD4**) structures in .pdb format are uploaded for docking with 7VFS_a and 7UHF proteins. A grid with dimensions x, y and z-coordinates (69.40, 66.94, 86.69) was generated at the active site of the 7VFS_a receptor. The list of calcium channel blocker drug molecules docking energies with the two N-type and L-type calcium channel receptor mole-

cules are listed in Table-2. Twenty drug molecules docking energies with 7VFS were in the range from -10.2 (efonidipine) to -6.1 kcal/mol (Amlodipine and nitrendipine) and with 7UHF are between -10.1 (amlodipine) to -6.3 (manidipine). The docked conformations and the type of interactions involved are represented in Figs. 2 and 3. The binding energies were in the range of -9.2 to 6.0 kcal/mol (7VFS) and -8.7 to 5.7 kcal/mol (7UHF) (Table-3). CD3 bound to the receptor with high binding affinity of -9.2 kcal/mol followed by KD3 with binding affinity of -8.7 kcal/mol. The amino acid residues of 7VFS_a protein LEU583, SER608, LEU660, THR661, ASN697, LEU700, LEU701, VAL1282, ILE1285, VAL1288, TYR1289, SER1362, THR-1363, VAL1401 to ASN1409, PHE1411 and SER1696 are involved in hydrogen bonding and other non-bonded interactions formation with the ligands (Fig. 2). The residues ARG-413, SER1008, PHE1110, ALA1140, PHE1150, GLN1156, GLU1157, LYS1161, ASN1165, LYS1170, ILE1455 and ILE-1456 of the protein 7UHF are forming non-covalent interactions in the docked complexes with the cilnidipine and its degradation products **CD1-CD3** and **KD1** and **KD3** molecules (Fig. 3). CD3, KD3 and KD4 are complexed with high binding affinities -8.7. -7.9 and -7.9 kacl/mol, respectively with 7UHF protein. The binding energies of cilnidipine and its degradation products were in the range of binding energies of the calcium channel blocker drugs (Table-3), conclude that the cilnidipine degradation products also showing similar strength of binding towards the receptor proteins with PDB ID 7VFS and PDB ID 7UHF.

TABLE-2
DOCKING RESULTS OF THE CALCIUM CHANNEL BLOCKER DRUGS WITH THE RECEPTOR PROTEINS PDB ID 7VFS AND PDB ID 7UHF

Drug molecule	Binding energy with N-type	Binding energy with L-type
Amlodipine	-6.1	-6.3
Aranidipine	-6.7	-6.7
Azelnidipine	-8.1	-9.1
Barnidipine	-8.6	-9.0
Benidipine	-8.8	-9.0
Clinidipine	-6.7	-6.4
Clevidipine	-7.1	-7.3
Efonidipine	-10.2	-9.7
Felodipine	-6.6	-7.1
Isradipine	-7.4	-7.3
Lacidipine	-6.6	-7.8
Lercanidipine	-9.1	-8.9
Manidipine	-9.7	-10.1
Nicardipine	-8.1	-8.0
Nifedipine	-6.4	-6.7
Nilvadipine	-6.8	-7.6
Nimodipine	-6.9	-7.0
Nisoldipine	-6.4	-7.1
Nitrendipine	-6.1	-7.4
Pranidipine	-7.6	-8.6

Structure confirmation

Conformational analysis: The degradants **CD1** and **CD2** with five stereocenters allow 16 diastereomers (two enantiomers of each **CD1** and **CD2** lead to a total of 32 stereoisomers). The

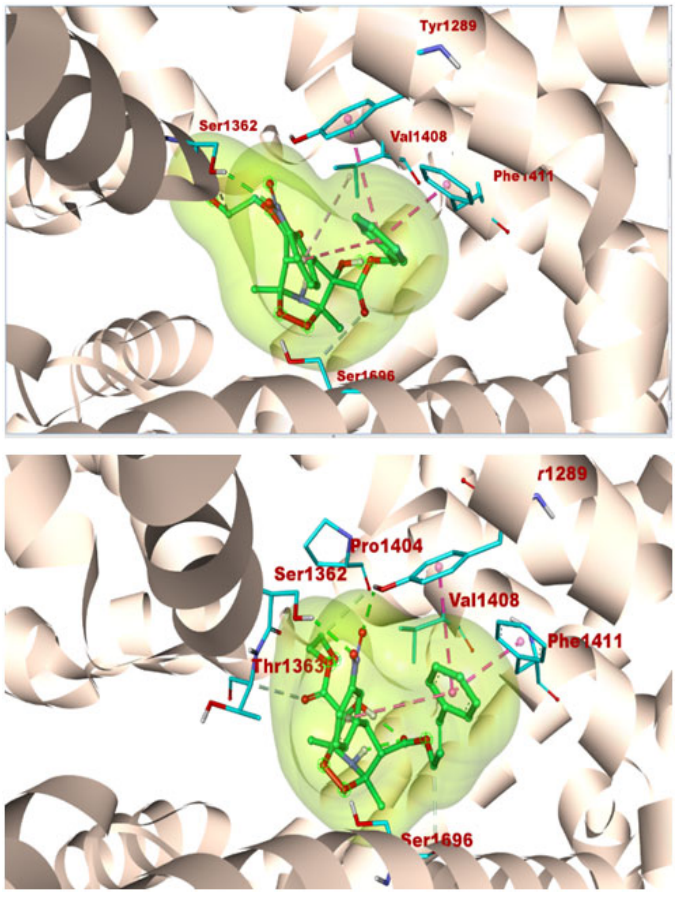

CD1

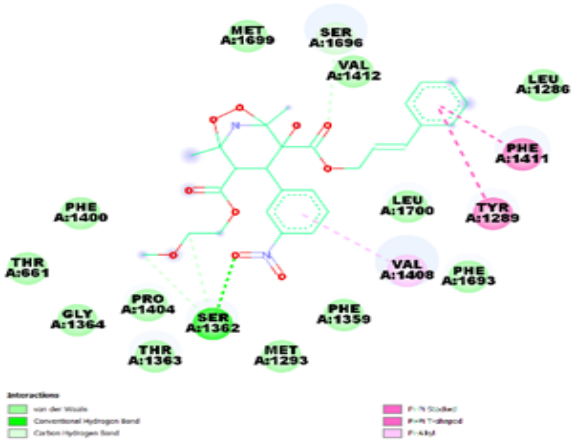

CD2

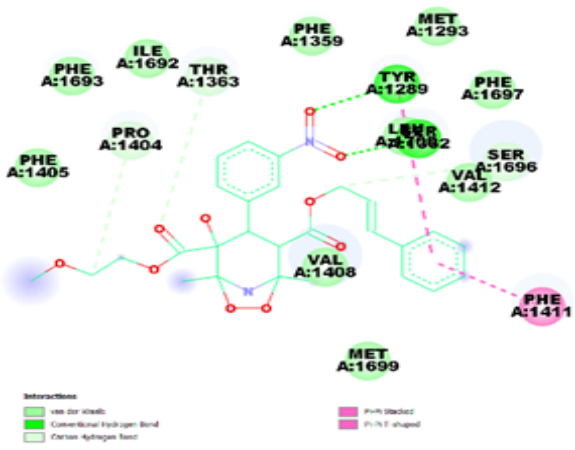

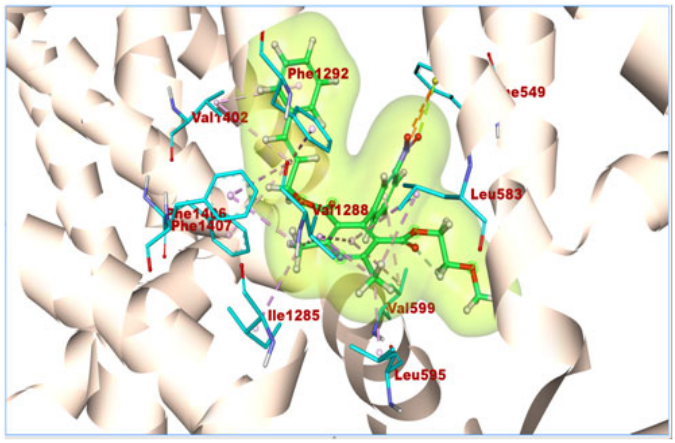

CD3

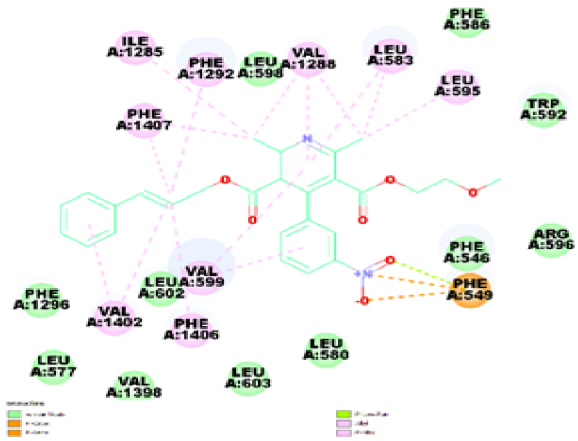

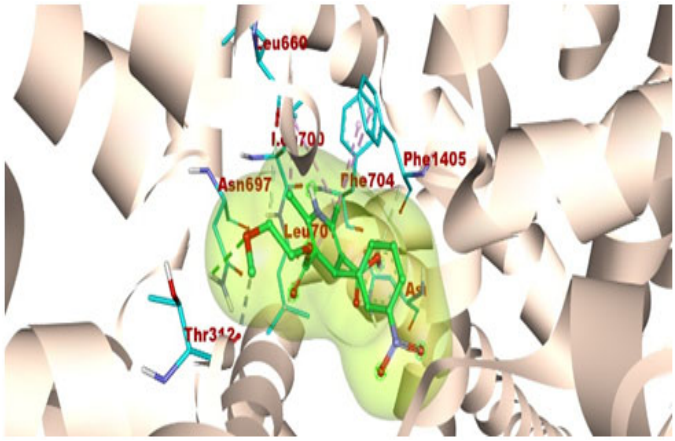

KD1

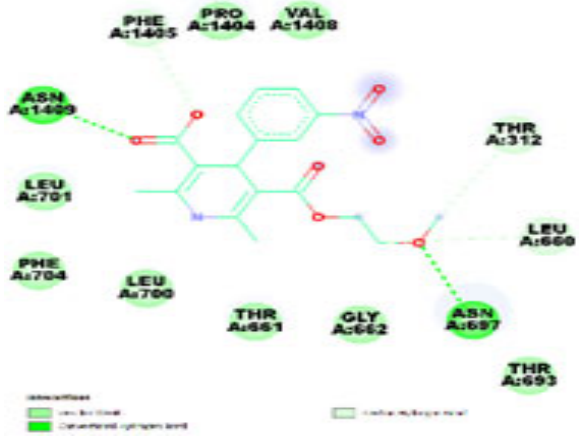

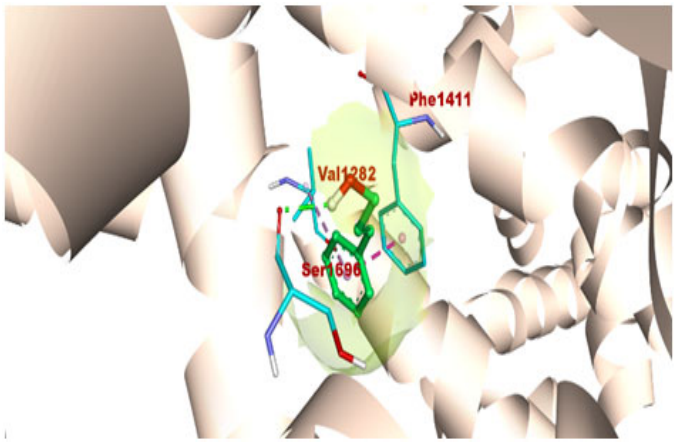

KD2

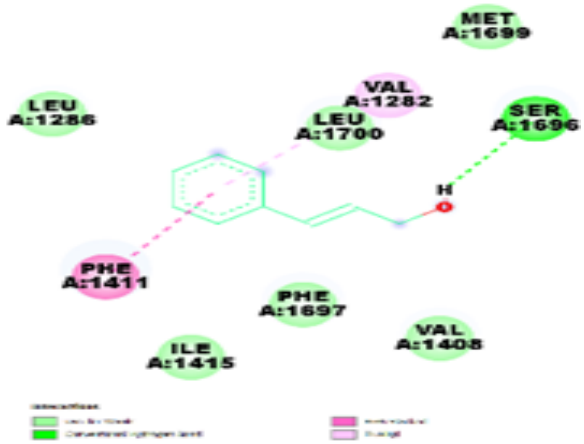

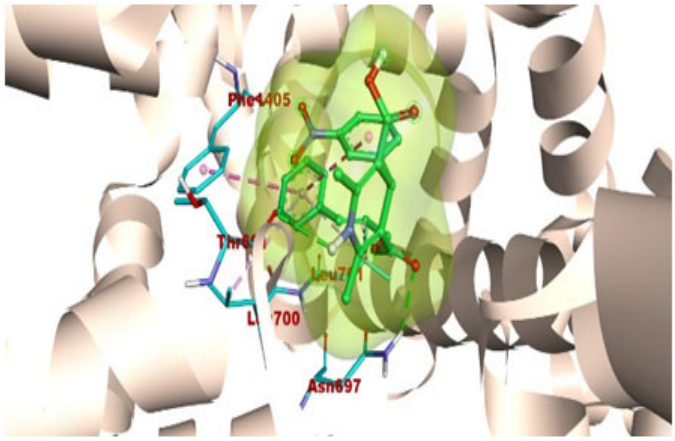

KD3

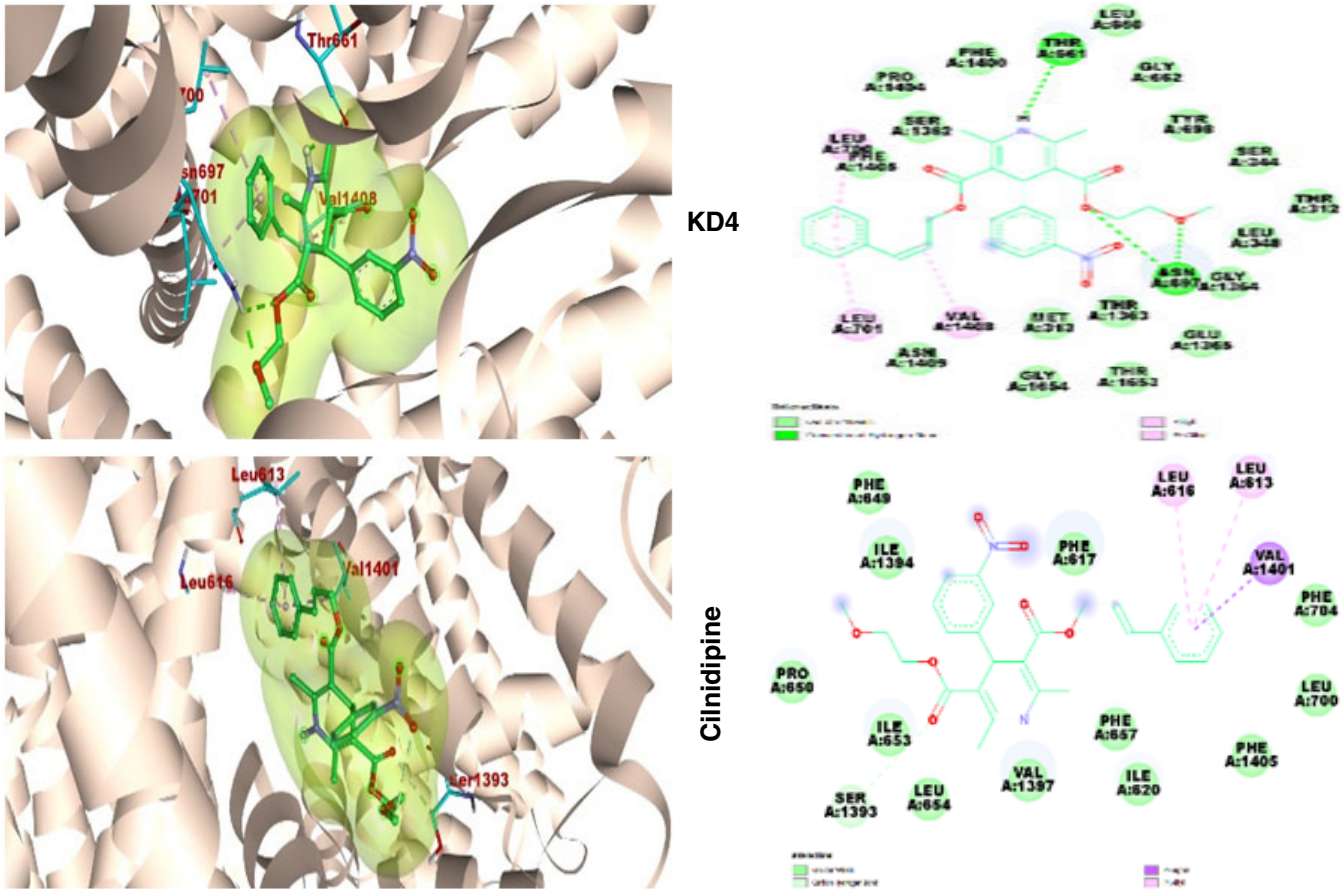

Fig. 2. Docked complexes of 7VFS along with cilnidipine molecule and degradation products **CD1-CD3** and **KD1-KD4**

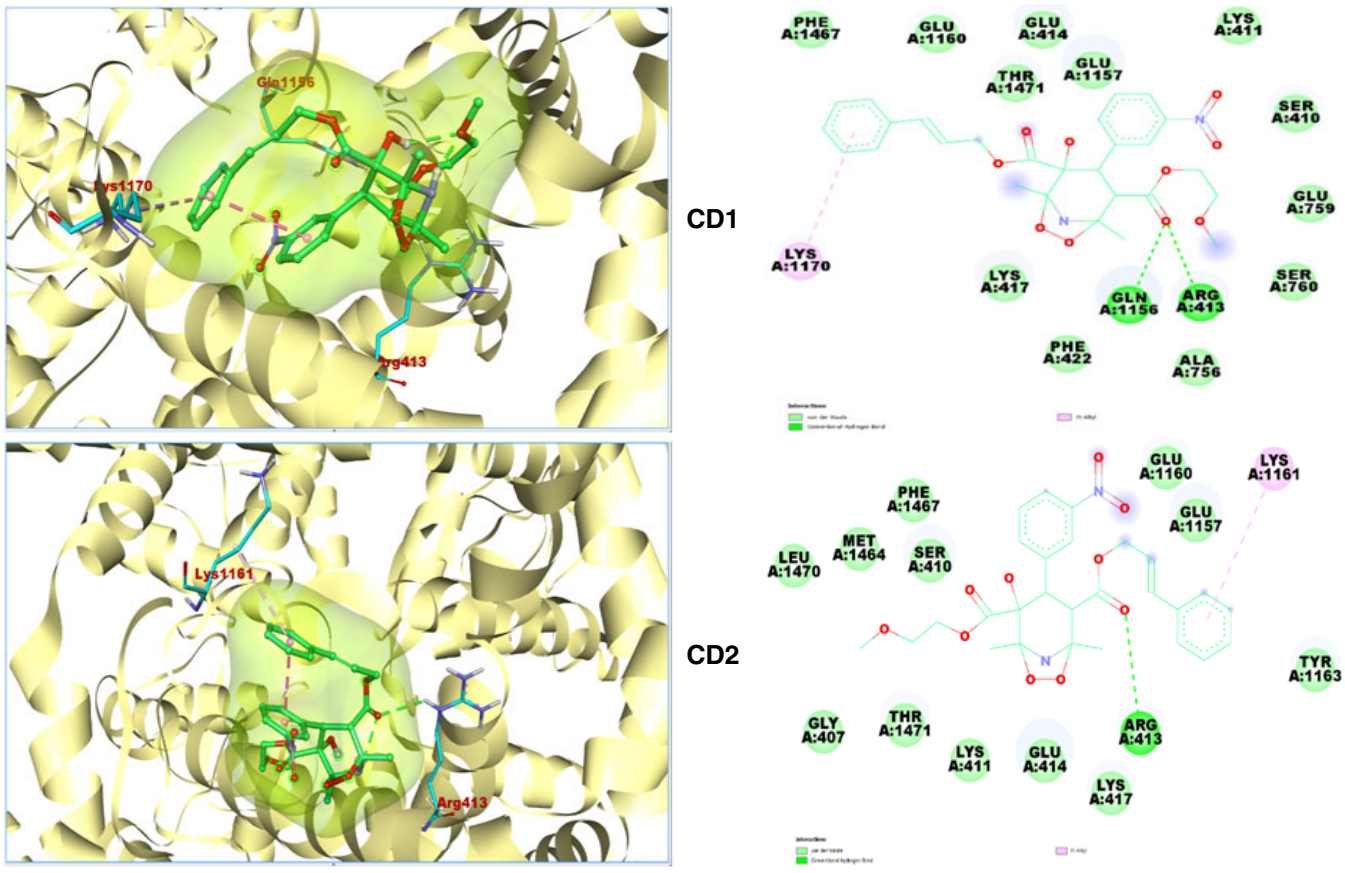

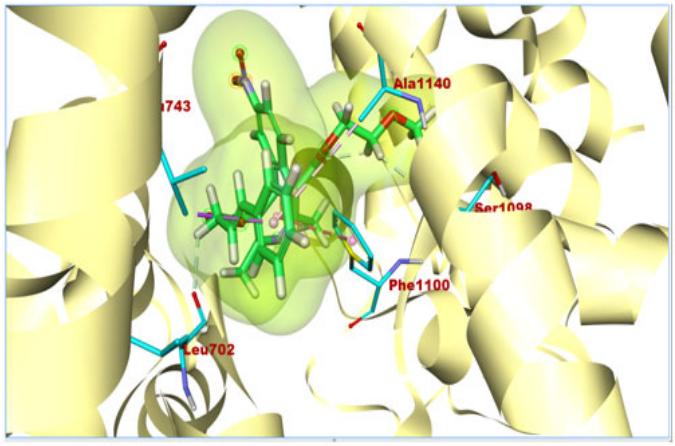

CD3

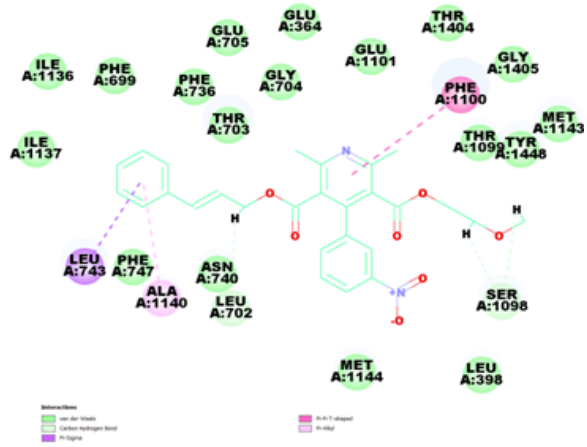

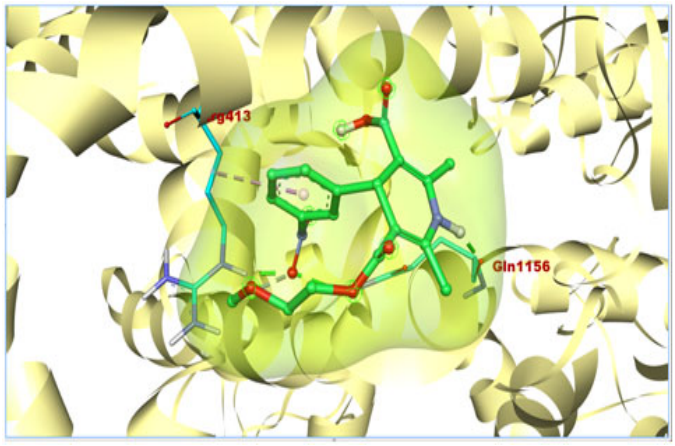

KD1

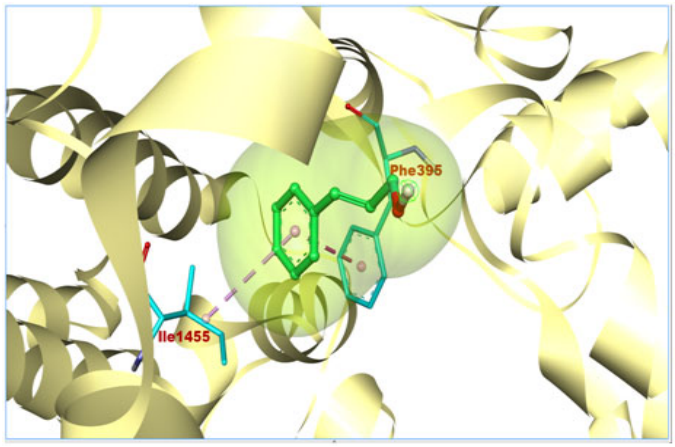

KD2

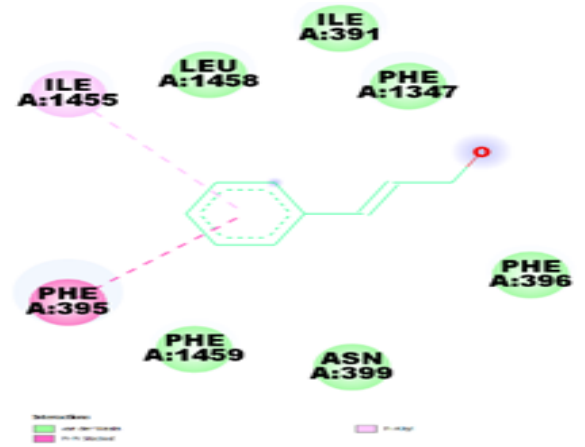

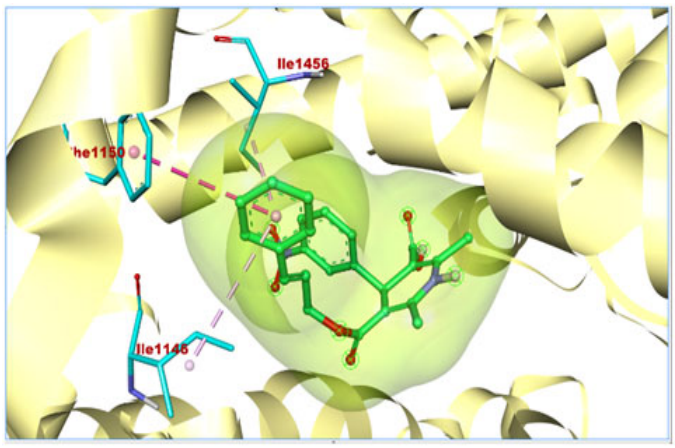

KD3

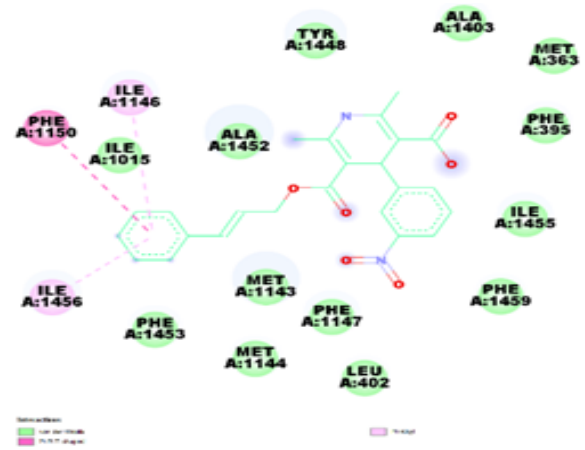

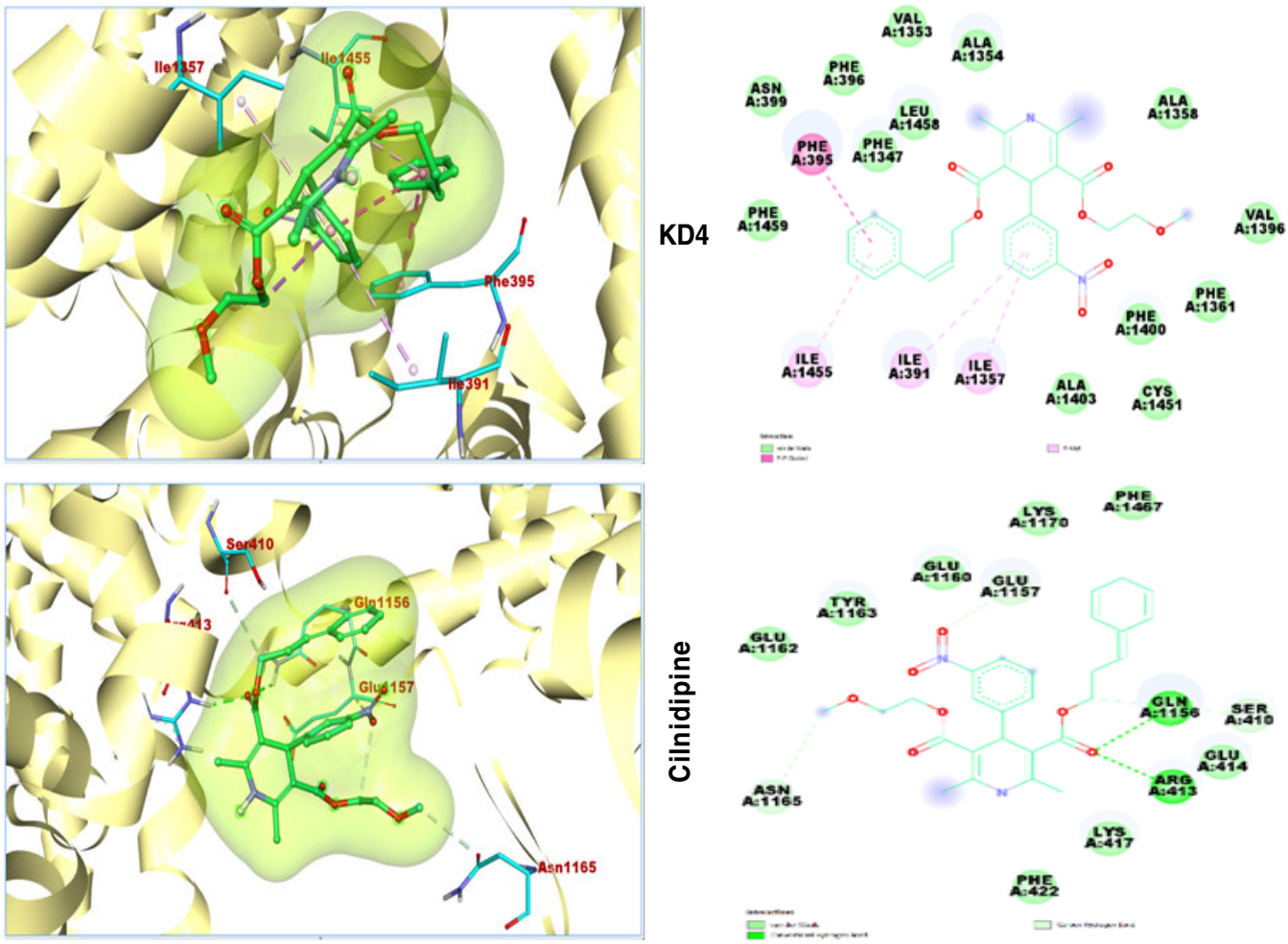

Fig. 3. Docked complexes of the protein PDB ID 7UHF with cilnidipine and its degradation products **CD1-CD3** and **KD1-KD4**

TABLE-3
BIDING ENERGIES (kcal/mol), MAIN DOCKING INTERACTIONS AND THEIR RESPECTIVE INTERACTION DISTANCES (Å) BETWEEN THE PROTEIN 7VFS (PDB ID) AND 7UHF AND THE DEGRADANTS ALONG WITH THE CILNIDIPINE. DOCKING INTERACTION TABLE: THE INTERACTIONS BETWEEN THE PROTEINS N-TYPE AND L-TYPE CALCIUM CHANNELS (PDB ID 7VFS AND 7UHF) AND THE CILNIDIPINE MOLECULE AND ITS DEGRADATION PRODUCTS (**CD1** TO **CD3** AND **KD1** TO **KD4**) ALONG WITH BOND DISTANCES ARE PRESENTED

Molecule	N-type Calcium Channel			L-type Calcium Channel		
	Binding energy	Interactions	Distance	Binding energy	Interactions	Distance
CD1	-8.0	Hydrogen bond		-7.8	Hydrogen bond	
		SER1696:CB-CD1:O	3.352		ARG413:HE-CD1:O	1.960
		CD1:C-SER1362:O	3.498		GLN1156:HE22-CD1:O	2.029
		CD1:C-SER1362:O	3.448		Pi-Alkyl	
		SER1362:HG-CD1:O	2.375		CD1-LYS1170	5.400
		Pi-Alkyl				
		CD1-VAL1408	4.809			
		Pi-Stack				
		PHE1411-CD1	3.868			
		TYR1289-CD1	4.885			
CD2	-8.4	Hydrogen bond		-7.5	Hydrogen bond	
		TYR1289:HH-CD2:O	2.169		ARG413:HE-CD2:O	2.785
		SER1362:HG-CD2:O	2.367		Pi-Alkyl	
		THR1363:CA-CD2:O	3.550		CD2-LYS1161	5.391
		CD2:C-SER1696:O	3.596			
		CD2:C-PRO1404:O	3.454			
		Pi-Pi stacking				
		PHE1411-CD2	4.024			
		TYR1289-CD2	4.991			

CD3	-9.2	Pi-Cation CD3:N34-A:PHE549 Pi-Anion CD3:O35-A:PHE549 Pi-Lone pair CD3:O36-A:PHE549 Alkyl A:VAL1402-CD3 CD3:C20-A:LEU583 CD3:C20-A:LEU595 Pi-Alkyl CD3:C20-A:VAL1288 CD3:C21-A:ILE1285 CD3:C21-A:VAL1288 A:PHE1292-CD3 A:PHE1406-CD3 A:PHE1407-CD3 A:PHE1407-CD3:C21 CD3-A:VAL1402 CD3-A:LEU583 CD3-A:VAL599 CD3-A:VAL1288 CD3-A:VAL599	 3.931 3.974 2.934 5.028 4.600 3.625 4.101 5.336 4.192 4.240 5.203 5.182 4.450 4.756 5.380 5.039 4.623 4.441	-8.7	Hydrogen bond CD3:H37-A:SER1098:O CD3:H41-A:SER1098:O CD3:H51-A:LEU702:O Pi-Pi T shape A:PHE1100-CD3 Pi-Alkyl CD3-A:ALA1140	 2.235 2.333 2.635 5.154 5.052
KD1	-6.7	Hydrogen bond ASN697:HD22-KD1:O ASN1409:HD21-KD1:O PHE1405:CA-KD1:O KD1:C-LEU660:O KD1:C-THR312:O Alkyl KD1:C-LEU700 KD1:C-LEU701 KD1:C-LEU700 Pi-Alkyl PHE704-KD1:C PHE1405-KD1:C	 2.840 2.173 3.771 3.753 3.613 4.458 5.216 4.159 5.073 4.625	-6.1	Hydrogen bond ARG413:HE-KD1:O GLN1156:HE22-KD1:O KD1:H-GLN1156:O Pi-Alkyl KD1-ARG413	 1.918 2.127 1.918 5.198
KD2	-6.0	Hydrogen bond KD2:H-SER1696:O Pi-Pi stack PHE1411-KD2 Pi-Alkyl KD2-VAL1282	 2.105 3.698 5.497	-5.7	Pi-Pi stacking PHE395-KD2 Pi-Alkyl KD2-ILE1455	 3.947 4.721
KD3	-8.7	ASN697:HD21-KD3:O KD3:H-THR661:O Pi-Pi Stack PHE1405-KD3 Pi-Alkyl KD3-LEU701 KD3-LEU700 KD3-LEU701	2.467 2.753 5.089 4.870 5.095 4.980	-7.9	Pi-Pi Stacking PHE1150-KD3 Pi-Alkyl KD3-ILE1146 KD3-ILE1456	 5.237 5.312 3.833
KD4	-8.3	Hydrogen bond ASN697:HD21-KD4:O ASN697:HD21-KD4:O KD4:H-THR661:O Alkyl VAL1408-KD4 Pi-Alkyl KD4-LEU700 KD4-LEU701	 2.477 1.890 2.488 4.719 5.214 4.900	-7.9	Pi-Pi Stacking PHE395-KD4 Pi-Alkyl KD4-ILE1455 KD4-ILE391 KD4-ILE1357	 4.018 4.875 5.230 5.136
Cilnidipine (CIL)	-6.7	Hydrogen bond SER1393:CB-CIL:O3 Pi-Sigma VAL1401:CG2-CIL CIL-LEU613 Pi-Alkyl CIL-LEU616	 3.797 3.515 5.203 5.161	-6.5	Hydrogen bond ARG413:HE-CIL:O GLN1156:HE22-CIL:O GLU1157:CA-CIL:O CIL:C-SER410:O CIL:C-ASN1165:OD1	 2.209 2.311 3.502 3.435 3.679

primary scope is narrowed to eight diastereomers by assuming a rigid *cis*-peroxy bridge with the piperidine ring. Although these degradants are rigid due to the *cis*-peroxy ring, several modes of conformational flexibility exist and need to be treated appropriately. Herein, the conformational mobility arose from (i) axial and equatorial conformations of core piperidine with N-H bond, (ii) nitro group of nitrophenyl can adopt two conformations and (iii) rotations of hydroxyl group. These flexibilities could generate 8 conformers for each diastereomer. However, it is shown that the N-H bond in equatorial position is stable than in the axial position by 0.72 kcal/mol [19]. This reduces to four conformations for each diastereomer. Surprisingly, many combinations were incompatible with certain stereochemical arrangements (*i.e.* some potential minimum energy conformers could not be located). For several diastereomers, only a single minimum energy conformer was located and the highest number of contributing conformers located for any one diastereomer was two. Also, for few of the diastereomers, multiple minimum energy conformers were located but were significantly higher in energy than the lowest energy minimum conformer. Hence, these conformers would not expect to contribute to the observed experimental spectrum.

However, it was decided to focus on eight diastereomeric structures for each of **CD1** and **CD2** as shown in Tables 4 and 5. The molecular geometries of these diastereomers were fully energy minimized at the B3LYP/6-31+G(d,p) level. The optimized geometries in its chair, boat and twist-boat confirmations, relative energies and the Boltzmann populations are presented in Table-4. Among the eight diastereomers of **CD1**, four attained chair (**CD1-2**, **CD1-3**, **CD1-4**, **CD1-8**), three attained boat (**CD1-5**, **CD1-6**, CD1-7) and one attained twist-boat (**CD1-1**) conformations with respect to the core piperidine ring. Among all the diastereomers, **CD1-2** in chair conformation is relatively more stable with 90.6% Boltzmann population followed by **CD1-8** which is 1.3 kcal/mole high in energy and with 9% Boltzmann population. The remaining six diastereomers are less stable by 3.1-11.3 kcal/mol with < 0.5% or 0% Boltzmann population (Table-4).

In case of **CD2**, three attained chair (**CD2-2**, **CD2-3**, **CD2-5**), two attained boat (**CD2-6** and **CD2-7**) and three attained twist-boat (**CD2-1**, **CD2-4** and **CD2-8**) conformations with respect to the core piperidine ring (Table-5). Among all these conformations, **CD2-3** (*SSRRR*) is relatively more stable with 100% Boltzmann weighted population. The remaining chair conformations in both the cases are destabilized due to the presence of diaxial repulsion between R_2 group and peroxy oxygen atoms. The boat and twist-boat forms are highly unstable by its nature. In addition, the hydrogen atom of NH in piperidine ring in both the degradants is oriented in the equatorial position, which is in good agreement with the earlier predictions [19].

The above conformational analysis narrowed the eight stereo configurations to two possible stereo configurations for each of the degradants **CD1** and **CD2**. The two identified configurations are **CD1-2** (*SSSRR*) and **CD1-8**, (*SSRSR*); and **CD2-3** (*SSRRR*) and **CD2-5** (*SSRSR*). Only these two configurations for each of **CD1** and **CD2** are used for the prediction of NMR chemical shifts. The remaining configurations are not considered due to their lesser stability.

^{1}H and ^{13}C NMR correlations: The geometries of stable conformations obtained above are subjected to GIAO calculations to obtain the ^{1}H and ^{13}C NMR chemical shifts in DMSO. As the geometry optimization of these degradants leads to a rigid structure, the rotational averaging of chemically equivalent protons is not represented in this type of calculations. Thus, different chemical shift for chemically equivalent protons were obtained using GIAO method. Therefore, in this work, the obtained values of chemically equivalent protons were averaged. The obtained statistical parameters for the correlation with the experimental chemical shifts for CD1 are presented in Table-6 for both the H and C nucleus. It was found that for **CD1**, the value of R^2 is close to unity with a negligible difference of 0.0052 and 0.0018 between the isomers of **CD1-2** and **CD1-8** for ^{1}H and ^{13}C correlations, respectively. Similarly, for the remaining statistical parameters like maximum absolute error (MaxE), the corrected mean absolute error (CMAE), corrected maximum absolute error (CMaxE) and RMSD, a negligible difference of 0.03, 0.05, 0.01 and 0.07 for ^{1}H and 0.48, 0.36, 2.52 and 0.21 for ^{13}C is observed between the isomers **CD1-2** and **CD1-8**, respectively. This small difference in all the statistical values between the isomers could not help to confirm the stereochemistry mainly at C2, C3 and C4 carbon atoms of the core piperidine ring. The stereochemistry at the C1 and C5 carbon atoms is assigned and fixed as *S* and *R* configuration (considering as one diastereomer) due to the rigid nature of the bridged peroxy group. In addition, the configuration at C3 can be *S* or *R* configuration as in the API is racemic mixture. Thus, considering only one enantiomer and fixing the configuration at C3 as *S* configuration where the nitrophenyl group is above the plane, the configuration at C2 and C4 needs to be assigned. For this, the steric effects which affects the stability of stereoisomer is considered. Therefore, it was found that there could be reduced electronic repulsions between the lone pairs of nitrogen and oxygen atoms if the OH group at C2 position of the core piperidine ring is present equatorially as in **CD1-2** configuration when compared to the OH group present axially as in **CD1-8**. This leads to assign the configuration at C2 as *S* configuration. Similarly, the bulky group R_2 at C4 atom needs to be in the equatorial position to reduce the steric interactions and this leads to assign the configuration as *R*. This arrangement of OH and R_2 group at C2 and C4 stabilized and made this stereoisomer as the global minima as seen from the relative energies (Table-4). Therefore, considering all the above observations, it is indeed suggested that **CD1** may well exist in **CD1-2** conformation and has stereo-configuration *S*,*S*,*S*,*R*,*R* at C1, C2, C3, C4, C5 chiral centres, respectively.

Similarly, in the case of **CD2**, the value of R^2 with respect to ^{1}H for **CD2-3** conformer is 0.9928, which is very close to unity when compared to **CD2-5** where the value is 0.9696. The remaining statistical correlation parameters of **CD2-3** are also very small compared **CD2-5**. Also, ^{13}C NMR correlation data is small for **CD2-3** conformation compared to **CD2-5**. Thus, ^{1}H and ^{13}C NMR correlations between the experimentally determined and theoretically predicted chemical shifts clearly

TABLE-4
RELATIVE CONFIGURATION AT THE CHIRAL CENTERS, OPTIMIZED CONFORMATION, RELATIVE ENERGIES (RE, kcal/mol) AND BOLTZMANN WEIGHTED POPULATIONS (BWP, %) FOR EACH OF THE DIASTEREOMERIC STRUCTURES OF **CD1** OBTAINED AT B3LYP/6-31+G(d,p) LEVEL

Structure	Relative configuration ($C_1C_2C_3C_4C_5$)	Optimized conformation		RE	BWP
CD1-1	*SSSSR*	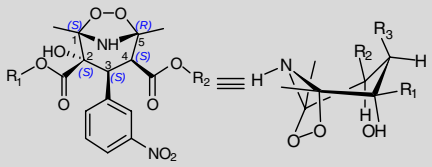	Twist Boat	10.7	0.0
CD1-2	*SSSRR*	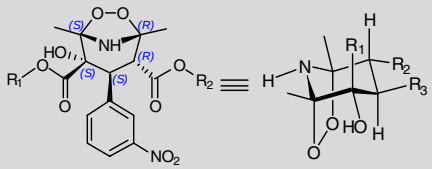	Chair	0.0	90.6
CD1-3	*SSRRR*	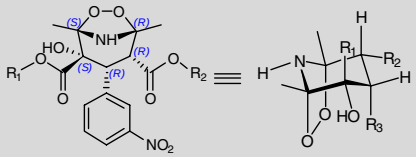	Chair	7.9	0.0
CD1-4	*SRRRR*	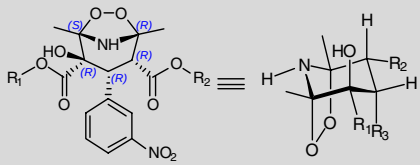	Chair	10.7	0.0
CD1-5	*SSRSR*	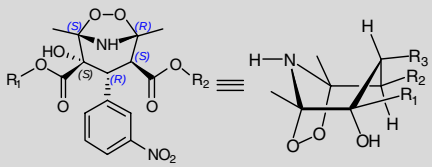	Boat	3.1	0.4
CD1-6	*SRSSR*	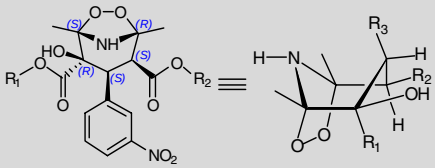	Boat	11.3	0.0
CD1-7	*SRRSR*	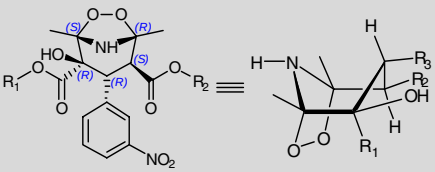	Boat	5.6	0.0
CD1-8	*SRSRR*	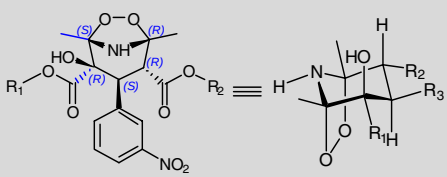	Chair	1.3	9.0

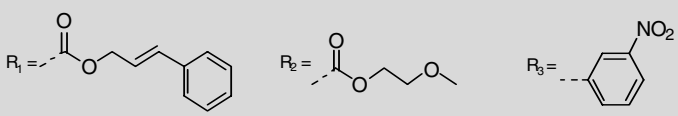

TABLE-5
RELATIVE CONFIGURATION AT THE CHIRAL CENTERS, OPTIMIZED CONFORMATION, RELATIVE ENERGIES (RE, kcal/mol) AND BOLTZMANN WEIGHTED POPULATIONS (BWP, %) FOR EACH OF THE DIASTEREOMERIC STRUCTURES OF **CD2** OBTAINED AT B3LYP/6-31+G(d,p) LEVEL

Structure	Relative configuration ($C_1C_2C_3C_4C_5$)	Optimized conformation		RE	BWP
CD2-1	*SSSSR*	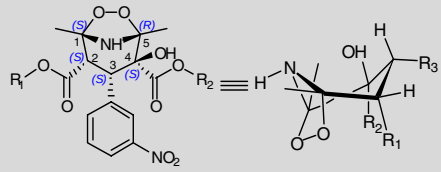	Twist Boat	13.8	0.0
CD2-2	*SSSRR*	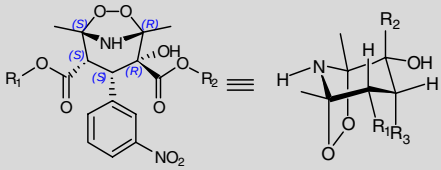	Chair	13.7	0.0
CD2-3	*SSRRR*	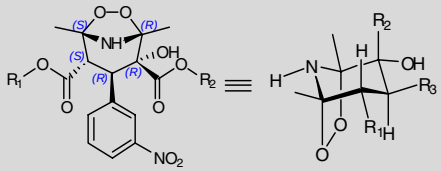	Chair	0.0	100
CD2-4	*SRRRR*	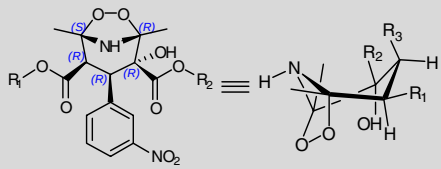	Twist Boat	13.8	0.0
CD2-5	*SSRSR*	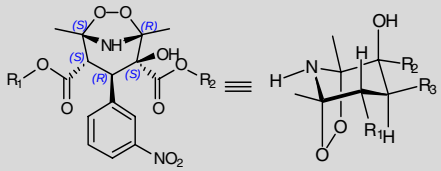	Chair	4.8	0.0
CD2-6	*SRSSR*	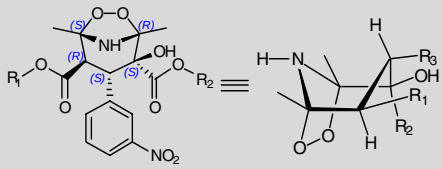	Boat	9.6	0.0
CD2-7	*SRRSR*	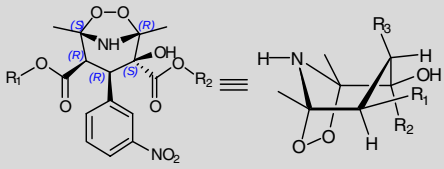	Boat	16.0	0.0
CD2-8	*SRSRR*	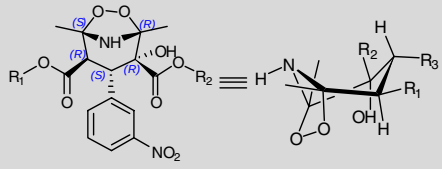	Twist Boat	7.1	0.0

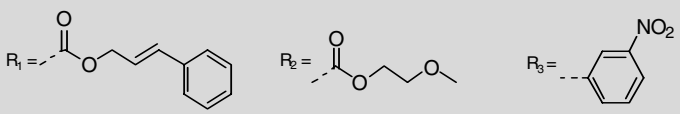

TABLE-6
STATISTICAL CORRELATION PARAMETERS FOR BOTH ^{1}H AND ^{13}C NMR OF STABLE CONFIGURATIONS OF **CD1** AND **CD2** USING THE CHEMICAL SHIFTS OBTAINED AT B3LYP/6-31+G(d,p) IN DMSO SOLVENT

Statistical parameter	δ_H		δ_C		δ_H		δ_C	
	CD1-2	**CD1-8**	**CD1-2**	**CD1-8**	**CD2-3**	**CD2-5**	**CD2-3**	**CD2-5**
a	-0.24	-0.14	4.94	6.15	0.06	0.04	5.17	6.54
b	1.1021	1.0614	0.9642	0.9509	1.0492	1.0659	0.9603	0.952
R^2	0.989	0.9832	0.9952	0.997	0.9928	0.9696	0.996	0.9946
MaxE	0.81	0.84	7.47	6.99	0.86	1.65	5.88	7.71
CMAE	0.16	0.21	2.32	1.96	0.15	0.25	2.19	2.47
CMaxE	0.68	0.67	7.56	5.04	0.48	1	5.71	7.9
RMSD	0.4503	0.3781	3.3625	3.1556	0.4009	0.5978	3.1684	3.8466

†a and b are the intercept and slope of the linear fitting line, respectively and R^2 is its correlation coefficient. MaxE is the maximum absolute error with respect to the linear fit. CMAE is the corrected mean absolute error and CMaxE is the corrected maximum absolute error. RMSD is the root mean square deviation.

suggests that the **CD2** may well exists in **CD2-3** configuration. Alternatively, the stereochemistry can be assigned by following the procedure as adopted for **CD1**. The stereochemistry at the C1 and C5 carbon atoms is assigned and fixed as *S* and *R* configuration; at C3 as *S* (nitrophenyl group is above the plane), the configuration at C2 and C4 needs to be assigned. To find the reduced electronic repulsions between the lone pairs of nitrogen and oxygen atoms, the OH group at C4 position of the core piperidine ring must be present equatorially as in **CD2-3** configuration when compared to the OH group present axially as in **CD2-5**. This leads to assign the configuration at C4 as *R*. Similarly, the bulky group R_1 at C2 atom needs to be in the equatorial position to reduce the steric interactions and this leads to assign the configuration as *S*. This arrangement of R_1 and OH groups at C2 and C4 stabilized and made this stereoisomer as the global minima as seen from the relative energies (Table-4). Therefore, considering all the above observations, it is indeed suggested that **CD2** may well exist in **CD2-3** conformation and has stereo configuration *S*, *S*, *R*, *R*, *R* at C1, C2, C3, C4, C5 chiral centres, respectively. In any case, the computationally assigned stereo-configuration is in good agreement with the experimental assignment using various NMR techniques [2].

Conclusion

The *in silico* toxicity and binding affinities of cilnidipine and its degradation products (**KD1** to **KD4** and **CD1** to **CD3**) were assessed. Among them four degradants (**KD1** to **KD4**) were predicted to be negative. Three degradants (**CD1** to **CD3**) are resulted positive, three degradants (**CD1** to **CD3**) need to be further studied in order to confirm the bacterial mutagenicity. The binding affinities were compared with 20 calcium channel blocker drugs along with the cilnidipine and its degradation products which are calculated against the protein PDB ID 7VFS are falling in the range between -10.2 to -6.6 kcal/mol and the protein PDB ID 7UHF were in the range between -10.1 to -5.7 kcal/mol. The interactions revealed the amino acid residues, which are involved in binding. Molecule **CD3** shows the highest binding affinity with the ligand molecules with binding energy -9.2 (kcal/mol) with 7VFS, -8.7 (kcal/mol) with 7UHF proteins and then **KD3** with binding energy -8.7 (kcal/mol) (7VFS) -7.9 (kcal/mol) (7UHF). Since **CD3** structure has alert group for bacterial mutagenicity, **KD3** can be considered as an effective molecule with more binding affinity across the degradation products. Finally, density functional theory (DFT) calculations were preformed to revisit the stereo-configuration around the five chiral carbon atoms present in **CD1** and **CD2**. The conformational analysis suggests that these degradants well exist in the stable chair conformation without steric interactions from the neighbouring groups. The availability of experimental ^{1}H and ^{13}C NMR spectra of one of its stereoisomers made us to carry out a direct comparison with the predicted values from DFT calculations without any empirical assumption. In this study, all the stereoisomers show subtle in their ^{1}H NMR, but significant differences in their ^{13}C NMR spectra, which were exploited for their structural assignment. Taken collectively the stable geometrical conformation and the small statistical parameters strongly suggests that the obtained degradation compounds prefer to exist in *S,S,S,R,R* and *S,S,R,R,R,* configurations at C1, C2, C3, C4, C5 chiral centers, respectively for **CD1** and **CD2**. The stereochemistry assignment was in good agreement with the experimental assignment using various NMR techniques. This comprehensive *in silico* approach significantly enhanced the understanding of bacterial mutagenicity, pharmacological activity and structural attributes of cilnidipine degradation products, serving as a valuable foundation for future experimental investigations.

ACKNOWLEDGEMENTS

The authors are thankful to Koneru Lakshmaiah Education Foundation management, the Management of United States Pharmacopeial Convention and Osmania University, Hyderabad, India for facilities and their immense support to publish this work.

CONFLICT OF INTEREST

The authors declare that there is no conflict of interests regarding the publication of this article.

REFERENCES

1. R. Yoshimoto, H. Dohmoto, K. Yamada and A. Goto, *Jpn. J. Pharmacol.*, **56**, 225 (1991); https://doi.org/10.1016/S0021-5198(19)39885-3

2. C. Krishnam Raju, J.V. Shanmukha Kumar and P.S. Kumar Goud, *New J. Chem.*, **42**, 634 (2018); https://doi.org/10.1039/C7NJ02781H
3. ICH M7(R1) - Assessment and Control of DNA Reactive (Mutagenic) Impurities in Pharmaceuticals To Limit Potential Carcinogenic Risk. (2018).
4. S.B. Ganorkar and Y.V. Heyden, *Trends Analyt. Chem.*, **157**, 116747 (2022); https://doi.org/10.1016/j.trac.2022.116747
5. N. Greene, K.L. Dobo, M.O. Kenyon, J. Cheung, J. Munzner, Z. Sobol, G. Sluggett, T. Zelesky, A. Sutter and J. Wichard, *Regul. Toxicol. Pharmacol.*, **72**, 335 (2015); https://doi.org/10.1016/j.yrtph.2015.05.008
6. C. Kim, T.G. Traylor and C.L. Perrin, *J. Am. Chem. Soc.*, **120**, 9513 (1998); https://doi.org/10.1021/ja981531e
7. O. Trott and A.J. Olson, *J. Comput. Chem.*, **31**, 455 (2010); https://doi.org/10.1002/jcc.21334
8. M.J. Frisch, G.W. Trucks, H.B. Schlegel, G.E. Scuseria, M.A. Robb, J.R. Cheeseman, J.A. Montgomery Jr., T. Vreven, K.N. Kudin, J.C. Burant, J.M. Millam, S.S. Iyengar, J. Tomasi, V. Barone, B. Mennucci, M. Cossi, G. Scalmani, N. Rega, G.A. Petersson, H. Nakatsuji, M. Hada, M. Ehara, K. Toyota, R. Fukuda, J. Hasegawa, M. Ishida, T. Nakajima, Y. Honda, O. Kitao, H. Nakai, M. Klene, X. Li, J.E. Knox, H.P. Hratchian, J.B. Cross, V. Bakken, C. Adamo, J. Jaramillo, R. Gomperts, R.E. Stratmann, O. Yazyev, A.J. Austin, R. Cammi, C. Pomelli, J.W. Ochterski, P.Y. Ayala, K. Morokuma, G.A. Voth, P. Salvador, J.J. Dannenberg, V.G. Zakrzewski, S. Dapprich, A.D. Daniels, M.C. Strain, O. Farkas, D.K. Malick, A.D. Rabuck, K. Raghavachari, J.B. Foresman, J.V. Ortiz, Q. Cui, A.G. Baboul, S. Clifford, J. Cioslowski, B.B. Stefanov, G. Liu, A. Liashenko, P. Piskorz, I. Komaromi, R.L. Martin, D.J. Fox, T. Keith, M.A. Al-Laham, C.Y. Peng, A. Nanayakkara, M. Challacombe, P.M.W. Gill, B. Johnson, W. Chen, M.W. Wong, C. Gonzalez and J.A. Pople, Gaussian 09, A.02; Gaussian Inc.: Wallingford CT (2009).
9. R. Ditchfield, *Mol. Phys.*, **27**, 789 (1974); https://doi.org/10.1080/00268977400100711
10. S. Miertu, E. Scrocco and J. Tomasi, *Chem. Phys.*, **55**, 117 (1981); https://doi.org/10.1016/0301-0104(81)85090-2
11. V. Barone and M. Cossi, *J. Phys. Chem. A*, **102**, 1995 (1998); https://doi.org/10.1021/jp9716997
12. A.D. Becke, *J. Chem. Phys.*, **98**, 5648 (1993); https://doi.org/10.1063/1.464913
13. K.L. Dobo, N. Greene, C. Fred, S. Glowienke, J.S. Harvey, R. Jolly, C. Hasselgren, M.O. Kenyon, J.B. Munzner, W. Muster, R. Neft, M.V. Reddy, A.T. White and S. Weiner, *Regul. Toxicol. Pharmacol.*, **62**, 449 (2012); https://doi.org/10.1016/j.yrtph.2012.01.007
14. M. Honma, *Genes Environ.*, **42**, 23 (2020); https://doi.org/10.1186/s41021-020-00163-1
15. R.V. Williams, A. Amberg, A. Brigo, L. Coquin, R. Jolly, A. Giddings, S. Glowienke, N. Greene, R. Kemper, C. O'Leary-Steele, A. Parenty, H.-P. Spirkl, S.A. Stalford, S.K. Weiner and J. Wichard, *Regul. Toxicol. Pharmacol.*, **76**, 79 (2016); https://doi.org/10.1016/j.yrtph.2016.01.008
16. T. Hanser, C. Barber, E. Rosser, J.D. Vessey, S.J. Webb and S. Werner, *J. Cheminform.*, **6**, 21 (2014); https://doi.org/10.1186/1758-2946-6-21
17. Y. Dong, Y. Gao, S. Xu, Y. Wang, Z. Yu, Y. Li, B. Li, T. Yuan, B. Yang, X.C. Zhang, D. Jiang, Z. Huang and Y. Zhao, *Cell Rep.*, **37**, 109931 (2021); https://doi.org/10.1016/j.celrep.2021.109931
18. A. Pandey, J. P, S. Tripathi and C. Gopi Mohan, *Mol. Inform.*, **31**, 643 (2012); https://doi.org/10.1002/minf.201200025
19. L. Carballeira and I. Pérez–Juste, *J. Comput. Chem.*, **19**, 961 (1998); https://doi.org/10.1002/(SICI)1096-987X(199806)19:8<961::AID-JCC14>3.0.CO;2-A